Non-Lambertian Photometric Stereo Based 3D-Reconstruction

{manchen2,anqiy1,huiy1}@andrew.cmu.edu

14 december 2017

1 Introduction

The Lambert's reflectance model is widely adopted in photometric stereo for its simplicity.However, the real world is full of non-Lambertian objects. Many photometric stereo algorithms have been developed to deal with non- Lambertian materials.

Let $\mathbf{I}_{P\times Q}$ denotes the observation matrix of P points under Q different lighting conditions; $\mathbf{N}_{P\times 3}^T$ denotes stacks of normal vector $n \in \mathbb{R}^{3\times 1}$; lighting vector $l \in \mathbb{R}^{3\times 1}$; $\rho(\mathbf{n},\mathbf{l})_{P\times Q}$ denotes the Bidirectional Reflectance Distribution Function values for each observation, which is a function of normal and lighting directions given viewing direction fixed at v = $(0,0,1)^T$; and 'o' denotes the element-wise multiplication. Then the non-Lambertian photometric stereo problem can be modelled as solve $\mathbf{N}$ from $\mathbf{I} = \max\left\{\boldsymbol{\rho}(\mathbf{n},\mathbf{l})o(\mathbf{N}^T\mathbf{L}), 0\right\}$ by using different assumptions and constrains on $\boldsymbol{\rho}(\mathbf{n},\mathbf{l})$.

In this project, we implemented three method. In section 2, we will introduce outlier rejection based model. In section 3, we will introduce analytic reflectance model. In section 4, we will introduce parametric BRDF Approximation. In section 5, we will present the experiment result and compare the results of the three methods.

2 Outlier rejection based model

2.1 Lambertian image formation model

Given n image with m pixels, we can define an observation matrix by aligning each image as a vector:

$$O = [vec(\mathbf{I}_1), ..., vec(\mathbf{I}_n)] \in \mathbb{R}^{m\times n} \tag{1}$$

where vec($\mathbf{I}_k$) for k = 1,...,n. $\mathbf{I}_k(j)$ is the image intensity in image K at point j

$$\mathbf{I}_k(j) = \rho_j \mathbf{n}_j^T \mathbf{l}_k \tag{2}$$

where $\rho_j \in \mathbf{R}$ is the diffuse albedo, $\mathbf{n}_j \in \mathbb{R}^3$ is the surface normal at the point and $\mathbf{l}_k \in \mathbb{R}^3$ describes the lighting direction. Therefore, the observations in a Lambertian scene can be expressed via the rank-3 expression

$$O = N^T L \tag{3}$$

where N = $[\rho_1 \mathbf{n}_1, ..., \rho_m \mathbf{n}_m] \in \mathbb{R}^{3\times m}$ and L = $[\mathbf{l}_1, ..., \mathbf{l}_n] \in \mathbb{R}^{3\times n}$

2.2 Non-Lambertian effects as sparse errors

In real scenes, various non-Lambertian effect are observed, like specularities, shadows, image noise and so on. We can interpret them as additive corruptions $\mathbf{E} \in \mathbb{R}^{m\times n}$ applied to an otherwise ideal Lambertian scene as

$$O = N^T L + E \tag{4}$$

Given observed images O and lighting directions L, out goal is to recover surface normals N in the presence of non-Lambertian corruption E. However, this is an under-constrained problem since the number of unknowns exceeds the number of linear equations. The overview of the method is as below. We applied a sparsity penalty to E, whose minimization reduce the infinity of feasible solutions to Eq.(4). Such penalty is based on the observation that non-Lambertian phenomena only emerge in limited areas of each image. Strictly speaking, we assume that the optimal feasible solution to Eq.(4) produces a sparse error matrix. Reflecting this assumption, the estimation problem can be formulated as

$$\min_{\mathbf{N},\mathbf{E}} ||E||_0 \ s.t. \ O = N^T L + E \tag{5}$$

Here, $||\cdot||_0$ is an l_0-norm penalty, which counts the number of non-zero entries in the matrix. If there exists imperfect lighting calibration or non-sparse specularities, then the above assumption are not true. In that way, the hard constraint in Eq.(5) is not appropriate ant more. To compensate for more diffuse modeling errors, we relax the hard constraint via an additional model mismatch penalty giving

$$\min_{\mathbf{N},\mathbf{E}} ||O - N^T L - E||_2^2 + \lambda ||E||_0 \tag{6}$$

where λ is a non-negative trade off parameter balancing data fit with sparsity. We consider Eq.(6) as an equivalent series of separate, pixel-wise optimization problem

$$\min_{\mathbf{x},\mathbf{e}} ||y - Ax - e||_2^2 + \lambda ||e||_0 \tag{7}$$

where y denotes an arbitary transposed row of O, A denotes corresponding $\mathbf{L}^T$, $\mathbf{x}$ is the associated unknown normal vector, and $\mathbf{e}$ is the sparse error component. Eq.(7) entails a difficult, combinatorial optimization problem that must be efficiently solved at every pixel. We apply a simple hierarchical Bayesian approximation to simultaneously estimate x and e. It is called Sparse Bayesian Learning.

2.3 Recovery of normals and corruptions via Sparse Bayesian Learning

Sparse Bayesian Learning assumes the standard Gaussian likelihood function for the first-level, diffuse error

$$p(\mathbf{y}|\mathbf{x},\mathbf{e}) = N(\mathbf{y}; A\mathbf{x}+\mathbf{e}, \lambda I) \tag{8}$$

Next, we apply independent, zero-mean Gaussian prior distribution on both $\mathbf{x}$ and $\mathbf{e}$:

$$p(\mathbf{x}) = N(\mathbf{x}; 0, \sigma_x^2 I) \tag{9}$$

$$p(\mathbf{e}) = N(\mathbf{e}; 0, \Gamma) \tag{10}$$

$\Gamma = diag[\gamma]$ is a diagonal matrix, where $\gamma = [\gamma_1, ..., \gamma_k]^T$ is a non-negative vector of variances in one-to-one correspondence with elements of e. A large variance γ_i indicates that the corresponding e_i is free to reflect the data, compensating for non-Lambertian effects, while a small or zero-valued variance implies that the associated error term is constrained near zero. In contrast, σ_x^2 describes the prior variance of the unknown normal vector; it is fixed to a large value to convey our lack of a priori certainty about x. Thus the prior on x will be relatively uninformative. Without prior knowledge as to the locations of the sparse errors, the empirical Bayesian approach to learning Γ is to marginalize the full joint distribution over all unobserved random variables, in this case x and e and then and then maximize the resulting likelihood function with respect to Γ. Equivalently, we will minimize

$$\begin{aligned} &L(\Gamma) = -logN(\mathbf{x}; 0, \sigma_x^2 I) \\ &\equiv log|\Sigma_y| + y^T \Sigma_{y_{-1}} y \\ &with \Sigma_y = \sigma_x^2 AA^T + \Gamma + \lambda I \end{aligned} \tag{11}$$

with respect to Γ. While L(Γ) is non-convex, the cost function from Eq.(11) is composed of two terms which are concave with Γ and the element-wise inverse of Γ respectively. Therefore, optimization can be accomplished building on a basic convex analysis that any concave function can be expressed as the minimum of a set of upper-bounding hyper-planes whose slopes are characterized by auxiliary variables. Thus, we can re-express both terms of Eq.(11) as a minimization over hyper-planes, where u are associated with the first term, and z are associated with the second. We first try to obtain a rigorous upper bound on the original cost function Eq.(11) characterized by u and z. For fixed values of z and u, there exists a closed form solution for Γ that incorporates the tighter bound. Likewise, for a fixed value of Γ, the auxiliary variables can be updated in closed form to tighten the upper bound around the current Γ estimate.This is a Expectation Maximum algorithm. The resulting update rules for the (k + 1)-th iteration are

given by

$$\begin{aligned}
&\gamma_i^{(k+1)} \rightarrow (z_i^{(k)})^2 + u_i^{(k)}, \forall i \\
&\Gamma^{(k+1)} = diag[\gamma^{(k+1)}] \\
&z^{(k+1)} \rightarrow \Gamma^{(k+1)}(S^{(k+1)})^{-1} y \\
&u^{(k+1)} \rightarrow diag[\Gamma^{(k+1)} - (\Gamma^{(k+1)})^2 (S^{(k+1)})^{-1}]
\end{aligned} \tag{12}$$

where $S^{(k+1)}$ is computed via

$$\begin{aligned}
&S^{(k+1)} = D - DA([\sigma_x^{-2} I + A^T D A])^{-1} A^T D \\
&D = (\Gamma^{(k+1)} + \lambda I)^{-1}
\end{aligned} \tag{13}$$

The above equations are guaranteed to reduce L(Γ) until a fixed point $\Gamma_*$is reached. Combining the likelihood and prior using Bayes' rule leads to the posterior distribution $p(\mathbf{x}, \mathbf{e}|\mathbf{y})/p(\mathbf{y}|\mathbf{x}, \mathbf{e})p(\mathbf{x})p(\mathbf{e})$. To estimate the normal vectors x, we may further marginalize over e to give

$$p(\mathbf{x}|\mathbf{y}) = p(\mathbf{x}, \mathbf{e}|\mathbf{y}) d\mathbf{e} = N(\mathbf{x}; \mu, \Sigma) \tag{14}$$

with mean and covariance defined as

$$\begin{aligned}
&\mu = \Sigma A^T (\Gamma + \lambda I)^{-1} \mathbf{y} \\
&\Sigma = [\sigma_x^{-2} I + A^T (\Gamma + \lambda I)^{-1} A]
\end{aligned} \tag{15}$$

We now have a closed-form estimator for x given by the posterior mean. The only issue then is the values for the unknown parameters Γ which we calculated before. This calculated Γ value can then be plugged into Eq.(15) to estimate the normal vector. We denote this point estimator as x_sbl. If the variances Γ_* reflect the true profile of the sparse errors, then x_sbl will closely approximate the true surface normal.

Now let's talk about the choice of λ and σ_x^2. The former can be reasonably set according to our prior expectations regarding the magnitudes of diffuse modeling errors, but in practice there is considerable flexibility here since some diffuse errors will be absorbed into e. In contrast, we can realistically set $\sigma_x^2 \rightarrow \infty$, which implies zero precision or no prior information about the normal vectors and yet still leads to stable, convergent update rules.However on certain problems a smaller σ_x^2 can lead to a modest improvement in performance, presumably because it has a regularizing effect that improves the convergence path of the update rules from Eq.(12).

3 Analytic Reflectance Model

Unlike the outlier rejection method that discards non-lambertian phenomena (including shadow and specular highlight) as outliers, analytic reflectance models fit a nonlinear analytic BRDF model to interpret all the observed data. In this section we introduce such a method that handles spatially-varying BRDFs by reconstructing surface shape and materials.

3.1 Analytic Relfectance Image Formation Model

Fundamental Materials Observation As is pointed out by Goldman et al.[24], real world variations in BRDF across a surface are often a result of the surface's composition from a small number of substances. These substances are therefore referred to as fundamental materials. The mixture status of these materials at each pixel are illustrated by a material weight maps. The color at pixel p of the observed intensity thus can be modeled as a convex combination of these basic materials:

$$I_{i,p,c} = \sum_m \gamma_{p,m} f_c(\mathbf{n}_p, \mathbf{L}_i, \alpha_m) \tag{16}$$

$I_{i,p,c}$ represents the intensity of channel c of pixel p in image i.The color channel c of the parameterized lighting model with normal $\mathbf{n}_p$, lighting condition $\mathbf{L}_i$ and BRDF parameter vector α_m together define the function f_c. Each fundamental material has a $\alpha_m.\gamma$ here denotes the whole material weight maps.

BRDF Modeling The isotropic Ward model [25] is used to model BRDF to keep the solution space highly constrained:

$$\rho_{bd,iso}(\theta_i, \phi_i; \theta_r, \phi_r) = \frac{\rho_d}{\pi} + \frac{\rho_s}{\sqrt{cos\theta_i cos\phi_r}} \frac{exp[-tan^2\delta/\beta^2]}{4\pi\beta^2} \tag{17}$$

Within this BRDF model, ρ_d is the diffuse reflectance coefficient,ρ_s is the specular reflectance coefficient, β is a measure of roughness, δ is the angle between $\mathbf{n}$ and the halfway vector $\mathbf{h} = (\mathbf{V} + \mathbf{L})/\|\mathbf{V} + \mathbf{L}\|$.There are seven parameters in this model. The parameter α_m of each fundamental materials corresponds to $\rho_{d,m}$,$\rho_{s,m}$ and β_m in this constructed model.The product of the BRDF component ρ and the lighting vector $\mathbf{L}$ gives the expression of f_c. We can drop the light intensity vector when computing f_c by normalizing the input image using the lighting vector.

Additional Constraints When using fundamental material maps to represent spatially-varying BRDF, the problem still remains underconstrained. The possibility of more-than-one combinations of basic materials that accurately describe most pixels introduces ambiguity to the model parameters. Two additional constraints of material priors are thus added to model to enforce feasible solutions.

The first constraints states that each pixel be described as a mixture of only two fundamental materials, since only the border regions require more types of pixel blending. This assumption has been proved to produce plausible results in experiments. The pairwise convexity constraint for the material weights are formulated as:

$$\gamma_{p,m} \geq 0, \sum_m \gamma_{p,m} = 1 \tag{18}$$

The second constraint enforces the fundamental materials to lie close to the space of observed materials, eliminating cases that an estimated material to be

far from any observed data in scene due to varying albedos. Thus a small spring term between each pair of fundamental materials is introduced to the model:

$$Q_{sp}(\alpha) = \sum_{i \neq j} \epsilon_d \|\rho_{d,i} - \rho_{d,j}\|^2 + \epsilon_s \|\rho_{s,i} - \rho_{s,j}\|^2 + \epsilon_\beta \|\beta_i - \beta_j\|^2 \qquad (19)$$

where (i, j) are all pairs of different materials.The values of ϵ_d and ϵ_s are set according to relative varying ranges of ρ_d and ρ_s. By empirical validation,the values are pre-set to $\rho_d = \rho_s = 1.0, \rho_d = 0.1$ for all examples.One thing to notice is that the spring term gives comparatively small values that only take effect when the observed intensity term alone can not give unique solution. This spring term does not imply that the fundamental materials should be similar to each other. It only constrains the fundamental materials to lie close to the observed data intensity.

The Image Model Combining the image model, the BRDF reflectance model, and the two constraints, the objective function is formulated as:

$$Q(\mathbf{n}, \alpha, \gamma) = \sum_{i,p,c} (I_{i,p,c} - \sum_m \gamma_{p,m} f_c(\mathbf{n}_p, \mathbf{L}_i), \alpha_m))^2 + Q_{sp}(\alpha) \qquad (20)$$

We aim to minimize Q with respect to the following unknowns: normals $\mathbf{n}$, material BRDF parameters α, and material weight maps γ.

3.2 Algorithm Optimization

In this sub-section we introduce the optimization procedure of the objective function given in (15).The steps are designed so the final solutions are more robust to local minima.Generally speaking, the system is designed to optimize the objective function iteratively by repeating the following steps:
(1) Optimize BRDF components while fixing the normals and material weights.
(2) Optimize surface normals and material weights while fixing the BRDF component.
(3) Enforce integrability of the normals generated in step (2).
Notice that step (3) is doing projection rather than optimization. This adjustment of normal estimates does only minor changes to the original values, which causes little impact to the objective function decreasing process.

Initialization The algorithm starts with initialization of normals and diffuse albedo using Lambertian photometric stereo.The initial material weight maps are computed using diffuse albedo transformed into HSV colorspace and discatd the V channel.

BRDF Component Optimization The objective function is optimized with respect to all BRDF parameters α simultaneously using the Levenberg-Marquardt nonlinear optimization algorithm.

Normals and Material Weight Map Optimization The normals $\mathbf{n}_p$ and weights maps $\gamma_{p,m}$ are optimized jointly. Firstly, we optimize weight maps by fixing normals. To this point, we can have the value of function f_c as the product of given lighting vector and estimated BRDF , using a discrete sampling of the estimated $\mathbf{n}$.The the weights $\gamma_{p,m}$ are computed by linear projection and brute force search over all normals and all pairwise combination of materials. Denote $\phi^c_{m,i}(\mathbf{n}_p) = f_c(\mathbf{n}_p, \mathbf{L}_i, \alpha_m)$, together with the constraint that $\gamma_{p,m1} + \gamma_{p,m2} = 1$,solving $\frac{dQ_p}{d\gamma} = 0$, we have

$$\gamma_{p,m1} \leftarrow \frac{\sum_{i,c}(I_{i,p,c} - \phi^c_{m2,i}(\mathbf{n}_p))(\phi^c_{m2,i}(\mathbf{n}_p) - \phi^c_{m1,i}(\mathbf{n}_p))}{\sum_{i,c}(\phi^c_{m2,i}(\mathbf{n}_p) - \phi^c_{m1,i}(\mathbf{n}_p))^2} \tag{21}$$

In order to accelerate the computation, the normal vectors are searched within normals that lie close to previously estimated normals. A final full global normal search is conducted after convergence to avoid trapping in local wrong directions.

Enforcing Integrability To obtain final result of 3D surface from the estimated surface normals, we need to ensure normal integrability. Let $\{n_x, n_y, n_z\}$ denotes normal for each point, the height field $z(x, y)$ is solved by minimizing

$$\Psi(z) = \sum_{x,y}(n_z\frac{\partial z(x,y)}{\partial x} + n_x)^2 + (n_z\frac{\partial z(x,y)}{\partial y} + n_y)^2 \tag{22}$$

We use conjugate gradient descent to solve this nonlinear equation.

4 Non-parametric BRDF Approximation

Photometric stereo algorithms capitalizing the general properties of BRDF have the potential to deal with much broader types of materials. In this section, we aim to introduce a general isotropic BRDF approximation method, which does not rely on any specific parameterized BRDF models and are purely dd-ata-driven". This algorithm is able to simultaneously estimate an independent surface normal at each point, a global set of BRDFs, and per-point material weights.

4.1 Image Formation Model

Bi-variate BRDF Assumption As is shown by Stark et al.[23], a general isotropic BRDF can be parameterized using two dimensional angles. This bivariate parameterization can be expressed by halfway/difference parameterization which is $\rho(\theta_h, \theta_d)$, where θ_i (the half angle) is the angle between the surface normal and the bisector of incident and exitant directions, and θ_d (the difference angle) is the angle between the source vector and the bisector vector.

Image Formation Model If we assume the BRDF at each point is linear combination of a set of basis BRDFs, then the BRDF at the i-th surface point

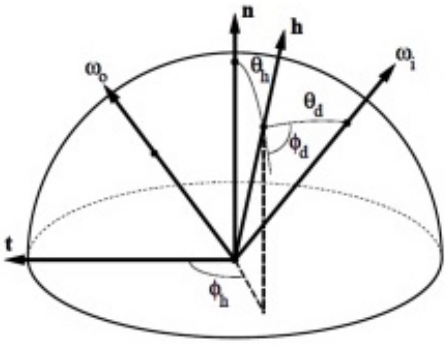

Figur 1: Bi-variate BRDF model

can be expressed as $\mathbf{H}_i^T = \mathbf{w}_i^T \mathbf{B}^T \in \mathbb{R}^{1\times d}$, where $\mathbf{w}_i \in \mathbb{R}^{k\times 1}$ is a set of material weights and $\mathbf{B} \in \mathbb{R}^{d\times k}$ contains a set of basis BRDFs. Then the image intensity of the i-th point under the illumination of j-th light source can be computed as,

$$\begin{aligned} e_{ij} &= \mathbf{H}_i^T \mathbf{\Phi}_{ij} max\{0, \mathbf{n}_i^T \boldsymbol{s}_j\} && (23)\\ &= \mathbf{H}_i^T \tilde{\mathbf{\Phi}}_{ij} && (24)\\ &= \mathbf{w}_i^T \mathbf{B}^T \tilde{\mathbf{\Phi}}_{ij} && (25) \end{aligned}$$

where $\mathbf{n}$ is the surface normal and $\mathbf{s}$ is the incident light vector, $max\{0, \mathbf{n}_i^T \boldsymbol{s}_j\}$ is the shading term ,and $\mathbf{\Phi} \in \mathbb{R}^{d\times 1}$ is an interpolation vector mapping the irradiance into the halfway/difference angle of measurement.

4.2 Alternating Constrained Least Squares

Given the image intensities matrix $\mathbf{E} \in \mathbb{R}^{n\times m}$, our goal is to simultoneously estimate three variables: (1)the material weight vectors at each point $\mathbf{W} = (\mathbf{w}_1, ..., \mathbf{w}_n)^T$, (2) a set of global BRDFs $\mathbf{B}$, (3) and the elevation angles of the surface normals. This can be formatted into a constrained least square problem with a target function,

$$\arg \min_{\mathbf{W},\mathbf{B},\mathbf{n}} \sum_{i=0}^{n} \sum_{j=0}^{m} \|\mathbf{w}_i^T \mathbf{B}^T \tilde{\mathbf{\Phi}}_{ij} - e_{ij}\|^2 \quad (26)$$

We can optimize the target function using alternating constrained least squares (ACLS), as is described by Lawrence et al.[12]. The optimization is done by alternatively updating $\mathbf{W}, \mathbf{n}$ and $\mathbf{B}$ to minimize the residuals. Specifically speaking, in each iteration, the weights $\mathbf{W}$ and the surface normal $\mathbf{n}$ are updated by fixing $\mathbf{B}$ and solving the convex optimization problem after which $\mathbf{B}$ is updated by fixing $\mathbf{W}, \mathbf{n}$ and solving the convex optimization problem. Note that global optimum w.r.t. weight $\mathbf{W}$ and surface normal $\mathbf{n}$ can be achieved simultaneously as the normal are constrained to have only one degree of freedom (elevation).

ACLS is guaranteed to reach local minimum as each iteration is guaranteed to not increase the residuals, but a global minimum cannot be guaranteed. Thus in practive one can do multiple random intialization for $\mathbf{W}, \mathbf{B}, \mathbf{n}$ in order to get an optimal solution.

4.3 Initialization

Our algorithm starts from recovering the azimuth angles of the surface normal by using Alldrin and Kriegman [1]. Then we randomly initialize the matrices $\mathbf{W}, \mathbf{B}$ and θ_n (the elevation component of the surface normal).

4.4 Update B with Fixed n and W

In order to optimize BRDF basis that minimize the L_2 error in the targe function, we set up the following sub problem,

$$\arg\min_{\mathbf{x}} \|\mathbf{A}\mathbf{x} - \mathbf{b}\|^2 \tag{27}$$

where $\mathbf{x} \in \mathbb{R}^{dk \times 1}$ is a vector encoding the entries of $\mathbf{B}$ in column-major order. $\mathbf{A}$ and $\mathbf{b}$ can be constructed as,

$$\mathbf{A} = \begin{pmatrix} \mathbf{A_1} \\ \vdots \\ \mathbf{A_n} \end{pmatrix} \tag{28}$$

$$\mathbf{A}_i = \mathbf{w}_i^T \otimes \tilde{\mathbf{\Phi}}_i^T \tag{29}$$

where $\otimes$ denotes the Kronecker product, and,

$$\mathbf{b} = \begin{pmatrix} \mathbf{b}_1 \\ \vdots \\ \mathbf{b}_n \end{pmatrix} \tag{30}$$

$$\mathbf{b}_i = \mathbf{E}_i^T \tag{31}$$

4.5 Update W and n with Fixed B

In this step, we first suppose $\mathbf{n}$ and $\mathbf{B}$ are both fixed. Then we are able to optimize the following function in order to get the optimal weights,

$$\begin{aligned} &\arg\min_{\mathbf{w}_i} \|\mathbf{A}_i\mathbf{w}_i - \mathbf{b}_i\|^2 \\ &\text{subject to,} \\ &\mathbf{w}_i \geq 0 \end{aligned}$$

where,

$$\mathbf{A}_i = \tilde{\mathbf{\Phi}}_i^T \mathbf{B} \quad \mathbf{b}_i = \mathbf{E}_i^T \tag{32}$$

with $\mathbf{E}_i = (e_2, ..., e_m)$ the set of measurements at the i-th surface point and $\tilde{\mathbf{\Phi}}_i \in \mathbb{R}^{d \times m}$ the corresponding interpolation matrix. Since the weights for each point are estimated independently, the computational complexity of this least square optimization is quite small. This enables us to compute the global optimum surface normal by exhaustively searching all possible $\mathbf{n}$ (only the elevation angle).

4.6 Additional Regularization

In practice, we found it necessary to impose smoothness and monotonicity on the BRDF domain, which can prevent specular highlights from dominating the solution. Our experiments show that these constraints help improve convergences as well as the visual quality of the recovered BRDFs.

Smoothness Constraint The smoothness constraint is motivated by the fact that specularities usually occur in a very compact region of BRDF domain, and within the domain BRDF value varies in orders of magnitude. This makes the region extremely sensitive to misalignment of light source; even a little misregistration can lead to large variation in intensity prediction. In order to relief this problem, we add a penalty term to our objective function. Let $\mathbf{D}_1 \in \mathbb{R}^{d \times d}$ be a discrete operator approximating the gradient over the BRDF domain. Then the penalty term can be formed as

$$\lambda_{D1}(\mathbf{D}_1\mathbf{B}_l)^T(\mathbf{D}_1\mathbf{B}_l), \text{for} \quad l = 1...k \tag{33}$$

Monotonicity Constraint It is quite simple to enforce monotonicity over a portion of the domain by only including inequalities from the desired subset of the domain. The monocity can be achieved by adding the following equality constraints:

$$B_{h,l} \geq B_{h+1,l}, \text{for} \quad l = 1...k \tag{34}$$

Monotonicity is particularly important in specular portions of the BRDF domain, where otherwise upsampling and registration error could cause unnatural visual artefacts in the recovered BRDFs.

5 Experiments

In this section, we compare the performance our three non-Lambertian photometric stereo algorithms on 'DiLiGenT' dataset.

5.1 Dataset

'DiLiGenT' dataset [4] is a benchmark dataset in non-Lambertian photometric stereo based 3D reconstruction. It contains ten objects, each of which is captured under the illumination of 96 white LED bulbs fixed on a rectangular frame. In terms of surface BRDFs, the dataset covers materials that are mostly difffuse

or with a rough surface, with strong and sparse specular spikes, with broad and soft specular lobes on uniform and spatial-varing materials, and with metallic paint on most uniform and spatial-varying surfaces.

5.2 Evaluation Criteria

Our evaluation is based on the statistic of angular error. For each pixel, the angular error is calculated as $\arccos(\mathbf{n}_0^{\mathrm{T}}\mathbf{n})$ in degrees, where $\mathbf{n}_0$ and $\mathbf{n}$ are 'ground truth' and estimated normals respectively. In addition to the mean angular error, we also calculate the minimum, maximum, median, the first quartile, and the third quartile of angular errors for each estimated normal map.

5.3 Experiment Results

We implemented and evaluated three algorithms - IW12[3], GC10[2], and AZ08[1], which are the landmark algorithms of outlier rejection method, analytic reflectance method and general isotropic BRDFs method respectively.

The evaluation results are summarized in Figure 2. It shows that IW2 performs well on objects including a dominant Lambertian component (BALL, CAT, POT1), but can not handle broad and soft specularity well. GC10, however, adopting a mixture of the Ward model, is able to achieve superior results on broad and soft specularity (POT2, COW). Its performances drops on objects with complicated spatially-varying BRDFs (GOBLET). The general isotropic BRDFs model AZ08 performs consistently moderate on all data, and outperforms other methods when the highlight is sparser and weaker (BALL, BEAR). More reconstruction results on the ten objects using these three algorithms are shown in the following figures.

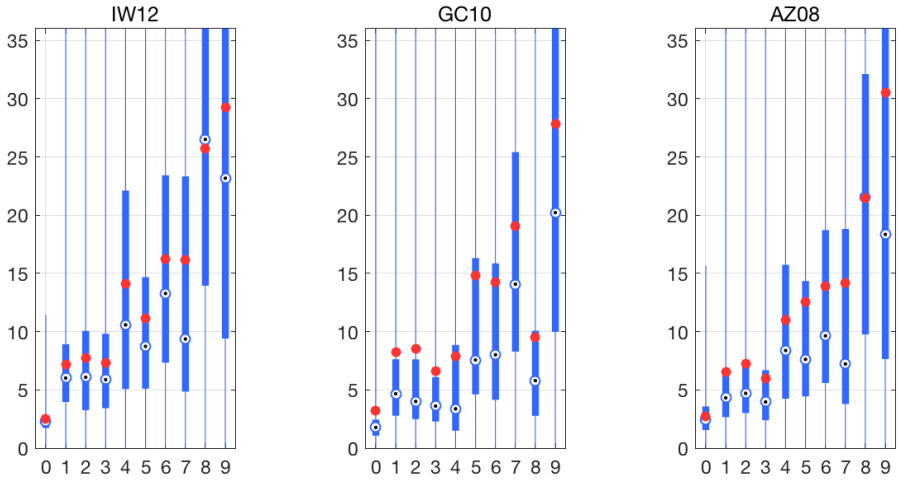

Figur 2: Angular errors of three landmark algorithms

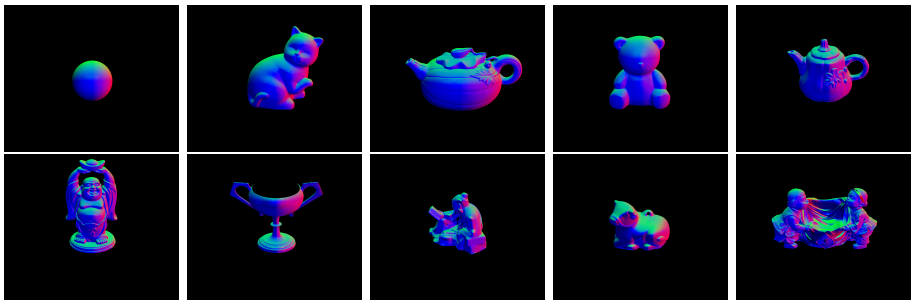

Figur 3: Estimated normal of ten objects using outlier rejection method IW12 [3]

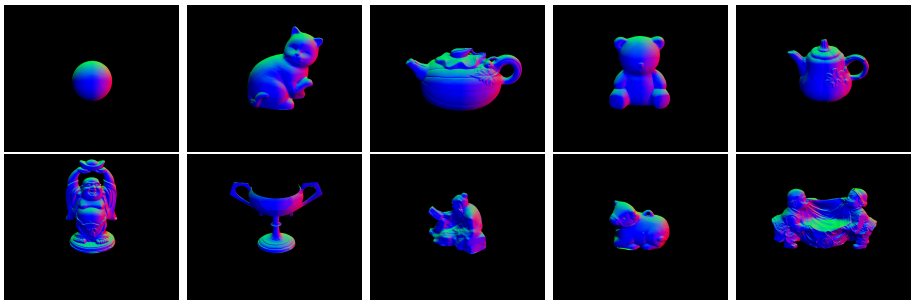

Figur 4: Estimated normal of ten objects using analytic reflectance model GC10 [2]

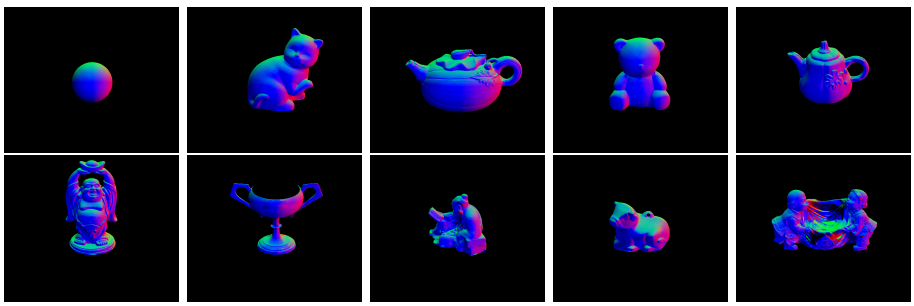

Figur 5: Estimated normal of ten objects using analytic reflectance model AZ08 [1]

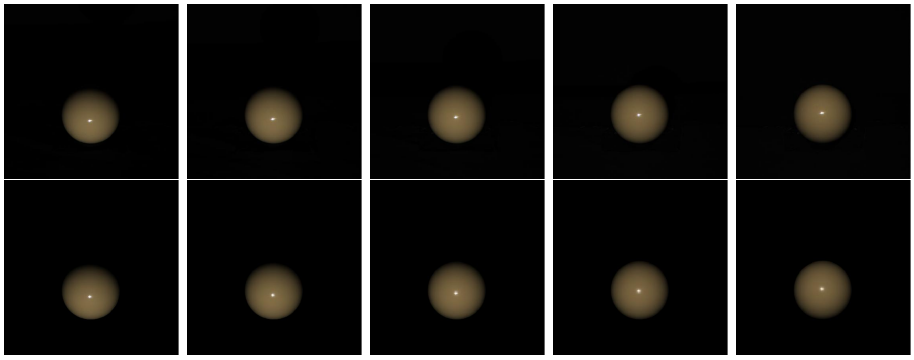

Figur 6: Original and reconstructed image of ball. The first row are the original image under different light source and the second row are the corresponding reconstructed image.

Figur 7: Original and reconstructed image of cat.

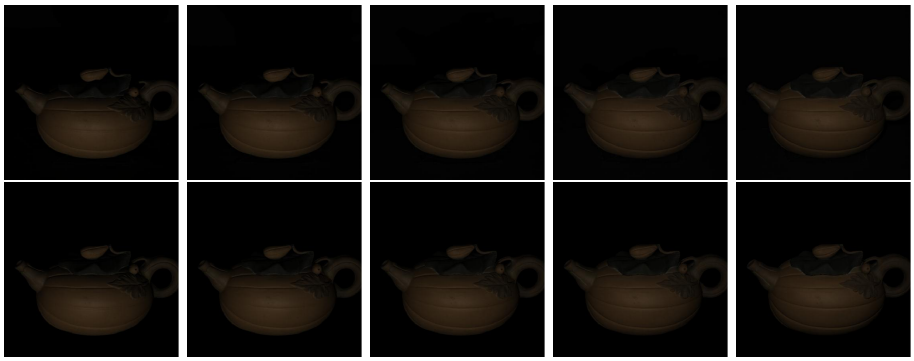

Figur 8: Original and reconstructed image of pot1.

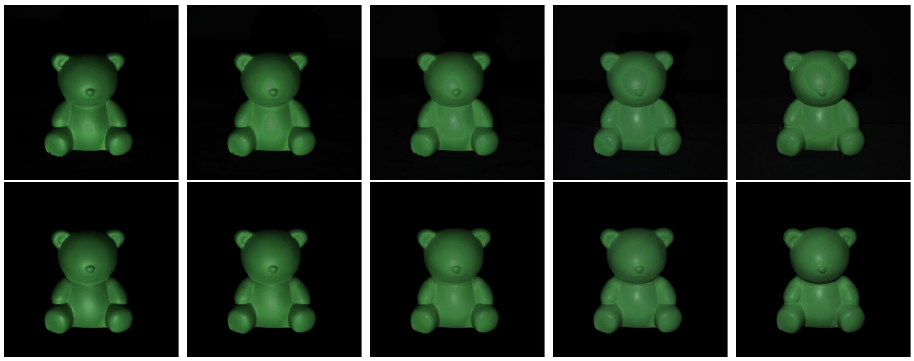

Figur 9: Original and reconstructed image of bear.

Figur 10: Original and reconstructed image of pot2.

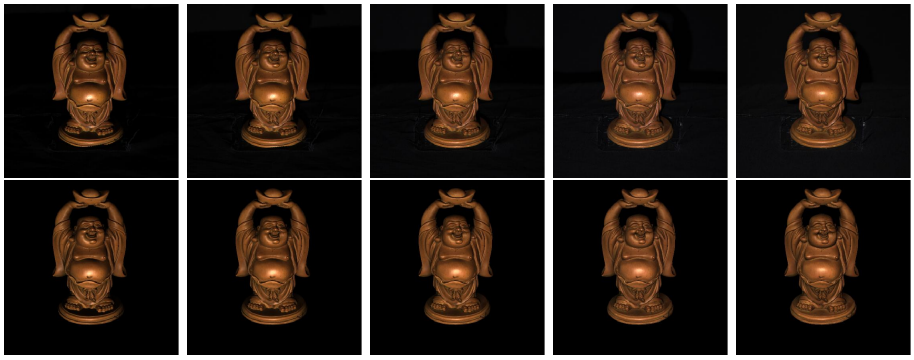

Figur 11: Original and reconstructed image of buddha.

Figur 12: Original and reconstructed image of goblet.

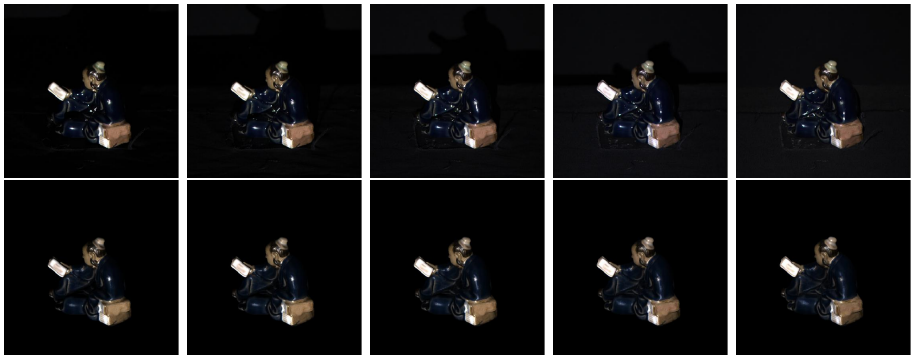

Figur 13: Original and reconstructed image of reading.

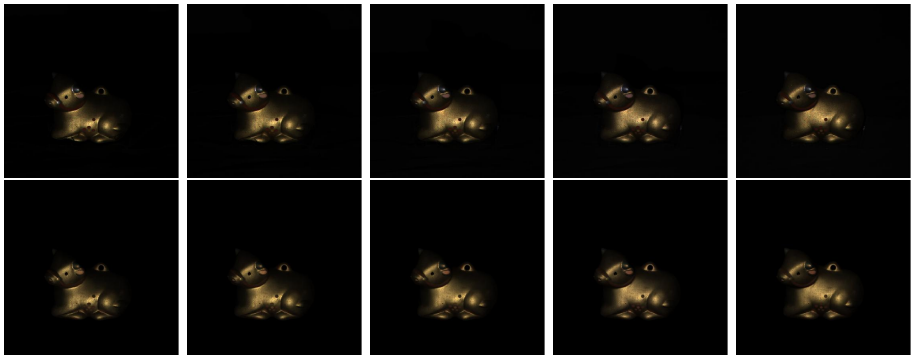

Figur 14: Original and reconstructed image of cow.

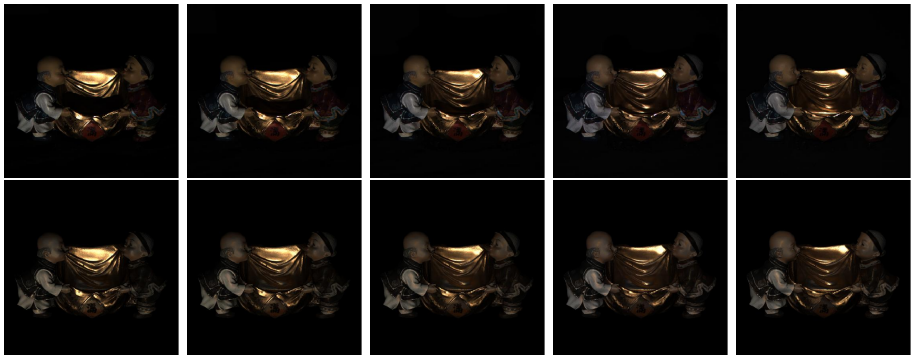

Figur 15: Original and reconstructed image of harvest.

Referenser

[1] Neil Alldrin, Todd Zickler och David Kriegman. “Photometric stereo with non-parametric and spatially-varying reflectance”. I: *Computer Vision and Pattern Recognition, 2008. CVPR 2008. IEEE Conference on*. IEEE. 2008, s. 1–8.

[2] Dan B. Goldman, Brian Curless och Aaron Hertzmann. “Shape and Spatially-Varying BRDFs from Photometric Stereo”. I: 1 (2005), s. 341 –348.

[3] Satoshi Ikehata m. fl. “Robust photometric stereo using sparse regression”. I: *Computer Vision and Pattern Recognition (CVPR), 2012 IEEE Conference on*. IEEE. 2012, s. 318–325.

[4] Boxin Shi m. fl. “A benchmark dataset and evaluation for non-lambertian and uncalibrated photometric stereo”. I: *Proceedings of the IEEE Conference on Computer Vision and Pattern Recognition*. 2016, s. 3707–3716.